Organic & Biomolecular Chemistry

Accepted Manuscript

This article can be cited before page numbers have been issued, to do this please use: X. Gan, G. Liu, M. Chu, W. Xi, Z. Ren, X. Zhang, Y. Tian and H. zhou, *Org. Biomol. Chem.*, 2016, DOI: 10.1039/C6OB02181F.

ROYAL SOCIETY OF CHEMISTRY

rsc.li/obc

DOI: 10.1039/C6OB02181F

Journal Name

ARTICLE

Intermolecular interactions boost aggregation induced emission in carbazole Schiff base derivatives

Received 00th January 20xx,
Accepted 00th January 20xx

DOI: 10.1039/x0xx00000x

www.rsc.org/

Xiaoping Gan [a, b], Guangjin Liu [a], Mingjie Chu [a], Wengang Xi [b], Zili Ren [a], Xiuli Zhang [a], Yupeng Tian [b], Hongping Zhou [b*]

Six D-π-A model compounds (Compounds **1-6**) were conveniently synthesized and characterized by ^{1}H NMR, ^{13}C NMR, MS and single crystal X-ray diffraction. One photon absorption and emission properties were studied by a series of UV-Visible and fluorescence spectra and theoretical calculations were applied to investigate the structure-property relationships, which showed that all the six compounds possessed obvious intramolecular charge transfer process which could be attributed to their optical properties. We simultaneously investigated their fluorescence emission performance in water/acetonitrile mixtures and found that they all owned outstanding aggregation induced emission properties. Scanning electron microscopy testing illustrated that orderly aggregation was the main cause for their aggregation induced emission properties. Cytotoxicity tests indicated that all these compounds had good biocompatibility for living cells, bio-imaging studies highlighted the potential application of the six compounds in one-photon fluorescence microscopy imaging domains.

Introduction

Organic molecules with strong fluorescence emission ability are useful as sensitizers for compound-sensitized solar cells (DSSCs), emitters for organic light emitting diodes (OLEDs) and stains for bio-imaging in a variety of applications. [1-3] An effective strategy to construct strong fluorescence emission organic molecules is to form a special structure patterns which own the electron donating group (Donor, D) linked an electron accepting group (Acceptor, A) by a π- bridge due to their strong absorption and emission properties originating from the intramolecular charge transfer (ICT) excitation from the donor to acceptor moiety of the dipole molecules. One of the noteworthy structural features of D - π - A molecules is that the electron density of the highest occupied molecular orbital (HOMO) is localized over the π - conjugated system close to the donor part, and that of the lowest unoccupied molecular orbital (LUMO) is localized over the acceptor part. Thus, the increase in the electron-donating abilities of donors and electron-accepting abilities of acceptors, respectively, leads to enhance the ICT progress and decrease the energy gap between the HOMO and LUMO, which could strengthen the fluorescence emission ability. [4] Moreover, choosing a different π-bridge will also influence the molecular conformation and then adjust the electron distribution to suit the requirements for optoelectronic devices, luminescent materials and bio-imaging applications. [5] For these reasons, a variety of such compounds which possessed D - π - A model have been synthesized and described in the literature, [6-8] including several stilbene derivatives. For example, Park and co-works reported that a series of highly fluorescent stilbene derivatives exhibit remarkable fluorescence properties. [9] Nevertheless, many of the D - π - A model molecules only emitted strong fluorescence in dilute solution but quenched the fluorescence in high concentration solution or in solid state, which limited their application in biological domain such as bio-imaging in living cells, because the environment in living cells is water soluble, which may induce organic molecules aggregating to quench the fluorescence. Thereby, the concept of aggregation induced emission (AIE), which was proposed by Tang and co-workers, [10] has been widely applied to develop the fluorescent biological stain. For instance, Neckers' group synthesized a cyano-stilbene derivative replaced by bis-carbazole groups showed obviously aggregation induced enhance emission (AIEE) and successfully applied to cell imaging. [11] Our group also focused on the development of organic fluorescent molecules with AIE properties and synthesized a series of D - π - A model triphenylamine Schiff base derivatives, [12] which owned different optical properties in aggregation state. We systematically studied their optical physical properties and found that the multiple weak interactions especially for C-H⋯π interactions played remarkable role in generating AIE performance in partial compounds, while some of these

[a] Department of Applied Chemistry, School of Science, Anhui Agricultural University, 230036 Hefei, P. R. China.
[b] College of Chemistry and Chemical Engineering, Anhui University and Key Laboratory of Functional Inorganic Materials Chemistry of Anhui Province, 230601, Hefei, P.R. China.
† Corresponding author. Fax: +86-551-63861279; Tel: +86-551-63861279
E-mail address: zhpzhp@263.net
Electronic Supplementary Information (ESI) available: [details of any supplementary information available should be included here]. See DOI: 10.1039/x0xx00000x

View Article Online
DOI: 10.1039/C6OB02181F

compounds showed aggregation quenching fluorescence (ACQ) due to π···π stacking between the adjacent molecules. The results illustrated that different aromatic rings would produce different weak interactions, which generated different influence on the luminescence performance under aggregation state.

Based on this, we utilized carbazole ring instead of triphenylamine as electron donor considering the carbazole ring possessed better planarity than the latter, which could produce more weak interactions originated from the aromatic rings. Meanwhile, carbazole is an electron-rich aromatic heterocycle with a nitrogen atom owned lone pair electrons which could be acted as electron donor. [13] Moreover, carbazole derivatives possessed high thermal stability, easy functionalization and excellent photophysical properties, which showed many potential applications in a variety of field. [14-16] In general, Schiff bases have strong coordination abilities with different coordination models, good biological activity and moderate electron withdrawing ability, so they are one of the effective candidates for the biological fluorescence probe. But pute Schiff bases possessed smaller conjugated system and lesser intramolecular charge transfer efficiency, thus constructing a Schiff bases derivative through appropriate π-bridge linked electron donating group to extend its conjugate system is expected to have more applications as luminescent materials. [17-18]

Herein, we designed and synthesized a series of D-π-A structure carbazole Schiff base derivatives (**Scheme 1**) containing carbazole as electron donating group and stilbene as π-bridge, simultaneously, adjusted their ICT progress through changing the structure of Schiff base moieties. Then we researched their linear optical properties in solutions and aggregation state through one photon absorption spectra (OPA) and one photon emission fluorescence spectra (OPEF), the results showed that all the six compounds owned AIE performance, but only compounds **1** and **6** possessed obvious fluorescence emission ability in solution, which illustrated the change of Schiff base' structure had significant influence on their luminescent ability. Furthermore, we discussed their structure - property relationship using crystal structure data and theoretical calculations, which revealed that the conformation of the molecules affected their emission properties even more. Meanwhile, the existence of the multiple weak interactions provided important impact for their optical properties at aggregation state. Finally, as expected, all the six compounds owned excellent living cell imaging abilities due to their good biocompatibility and suitable AIE properties. So we successfully explored the application of the six compounds in bio-imaging.

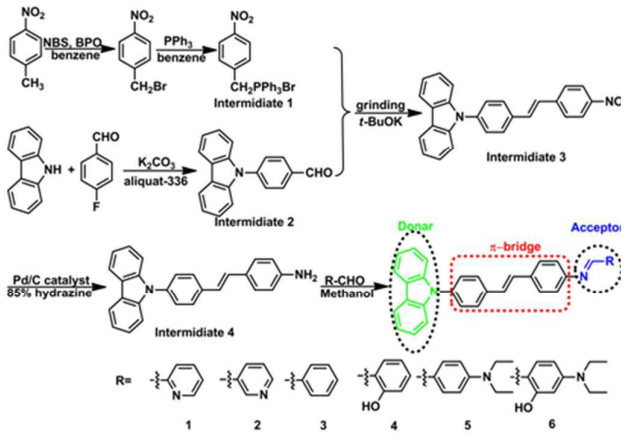

Scheme 1. Synthetic routes of compounds **1-6**.

Results and discussion

1 Synthesis

Six compounds were prepared according to the synthetic routes showed in **Scheme 1**. The experiment details and structure characterization data were described in the experimental section and electronic supporting information (ESI).

2 Crystal structures

To investigate the structure - property relationship of the synthesized compounds, we elucidated the molecule structure in solid state. Fortunately, the single crystal of compounds **1, 2, 3, 5** and **6** were obtained by slow evaporation from dichloromethane and ethanol mixture solution. Their molecular structure diagrams with atom numbering scheme and stacking structures involved some weak interactions among the adjacent molecules were depicted in **Figs. 1-3**. The crystallographic data were summarized in **Table S1**. From the **Fig. 1a**, we could see that the compound **1** maintained good planarity at the styrene π- bridge with a dihedral angle (θ_2) between the plane (P1) consisted with C13, C14, C15, C16, C17, C18, C19 and the plane (P2) of C21, C22, C23, C24, C25, C26 was 10.186(98)°, the bond length of the π - bridge in compound **1**, including C16-C19, C19=C20 and C20-C21, was 1.474(4) Å, 1.324(5) Å and 1.470(4) Å, respectively, which meant there existed good delocalization system in the section of these compounds. Whereas the dihedral angle (θ_1) between the carbazole plane and the plane P1 was 62.274(74)°, and the dihedral angle (θ_3) between the terminal pyridine ring (P3) and the plane P2 was 52.885(101)°, which indicated that the donor (carbazole ring) and the acceptor(pyridine Schiff Base moieties) deviated the plane of the styrene resulting in a poor planarity in whole molecule. Why not the donor and acceptor were coplanar with the styrene π - bridge? One reason for the structure feature was that the existence of intramolecular hydrogen bond (C30-H30···N2, *d* = 2.463 Å, ∠C30-H30-N2 = 100.786(394)°) restricted the rotation of the pyridine ring around the carbon-carbon single bond(C28-C29), Another reason could be seen from the stacking structures which showed in **Fig. 1b**. we could see that the intermolecular interactions including a rare but reasonable H···H interaction [19-21] (H11···H32, *d* = 2.354(53) Å, in which H11 located at electron-rich carbazole ring owning high electron cloud density and H32 located at electron-poor pyridine ring owning low

View Article Online
DOI: 10.1039/C6OB02181F

electron cloud density) and C-H···π weak interaction (C22-H22···π, *d* = 2.201(23) Å), played significant role in the growth of 1D chain along *a*-axis, especially for the H···H interactions, which not only connected two adjacent molecules into a dimer adopting *J*-aggregation with a head to tail model, but also restricted the rotations of the two terminal aromatic ring around the single bond, respectively. We also cautiously calculated the H···H interaction's energy through theoretical calculation based on the crystal structure and the result was 28 KJ.mol^{-1}, which located in the normal range of the weak interactions [22-25] and further illustrated the rationality of its existence. As a result, the whole molecule owned a non-planar conformation and prevented the formation of the π···π stacking. Then the 2D layer structure formed through C-H···π weak interactions (C2-H2···π, d = 2.702(38) Å) which generated from the C-H of carbazole ring with another carbarzole ring in the adjacent molecule (**Fig. 1c**). All the results illustrated that the carbazole unit had an important control function on the molecule stacking structure.

Similar with compound **1**, compounds **2** and **3** possessed uniform molecule configuration. The dehydral angle (θ_1) was 13.270(139)° for compound **2**, 8.006(129)° for compound **3**, the dehydral angle (θ_2) was 58.199(104)° for compound **2**, 59.134(108)° for compound **3**, and the dehydral angle(θ_3) was 39.404(182)° for compound **2**, 36.185(159)° for compound **3**, respectively.

Different with compound **1**, **2** and **3**, compound **5** and **6** owned a distinct molecule configuration which was showed in **Fig. 2**. We could see that the styrene section in compounds **5** and **6** were non-planar with a large dihedral angle (θ_1) of 29.396(201)° and 32.399(142)°, respectively. While the dihedral angle (θ_3), (0.618(222)° for compound **5** and 11.644(110)° for compound **6**) were smaller than that in compounds **1**, **2** and **3**, which illustrated the Schiff base moieties maintained good planarity with the plane of P2. The result stated that different acceptors had outstanding influence on the molecule configuration, especially for the molecule planarity. The stacking structures of compounds **2, 3, 5** and **6** were illustrated in **Fig. 3**. We could see that they were all different with the compound **1** that there was inexistence of the strong H···H interactions which could connect two adjacent molecules to a dimer. The absence of the H···H interactions resulted in the free rotation of the terminal groups in these molecules.

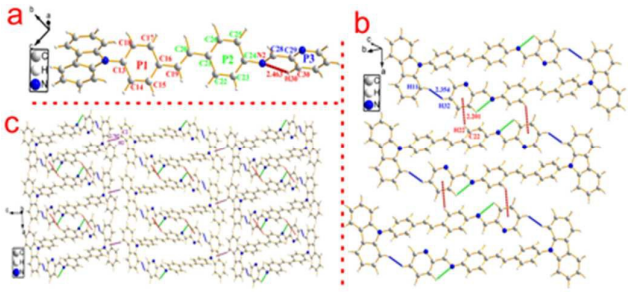

Fig.1 Crystal structure of compound **1** (a) Single molecule, (b) 1D chain structure and (c) 2D layer structure.

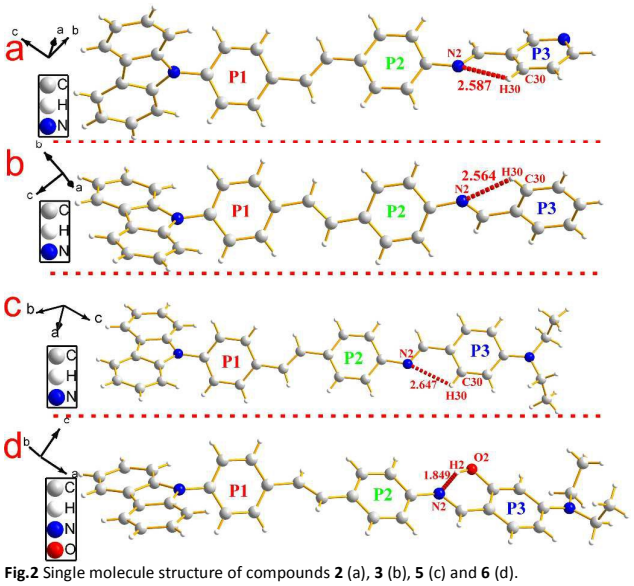

Fig.2 Single molecule structure of compounds **2** (a), **3** (b), **5** (c) and **6** (d).

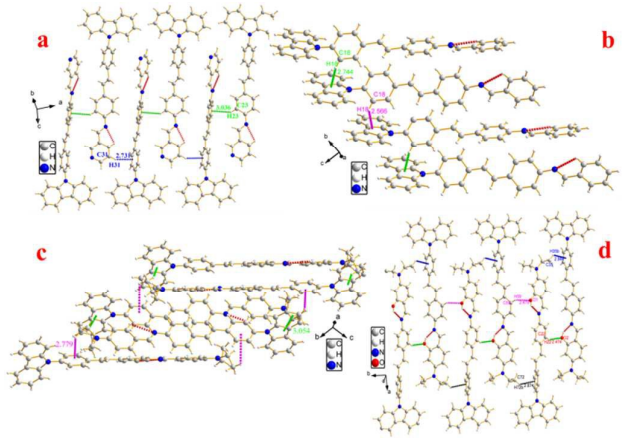

Fig.3 2D chain structure of compounds **2**(a), **3**(b), **5**(c) and **6**(d).

3 One-photon absorption and emission properties

The One photon absorption and fluorescence emission spectra of compound **1** in six solvents of varying polarities

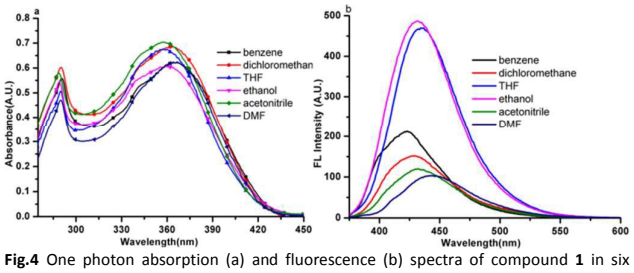

Fig.4 One photon absorption (a) and fluorescence (b) spectra of compound **1** in six organic solvents of different polarity with a concentration of 1 × 10^{-5} mol. L^{-1}.

View Article Online
DOI: 10.1039/C6OB02181F

were depicted in **Fig.4**. The absorption spectra of the other five compounds (**2-6**) were depicted in **Figs. S2-6**. It could be seen from **Fig. 4a** that compound **1** had two absorption peaks located at ~280 nm and ~360 nm, the former was assigned to the π-π* electronic transitions caused by the carbazole core [26] whereas the latter is likely ascribed to intramolecular charge transfer between the carbazole ring and the terminal Schiff base group. From the **Figs. S2-6**, it could be seen that the other five compounds had similar feature in absorption spectra.

The fluorescence spectra showed obvious difference from compound **1** to **6.** It could be seen from **Fig. 4b & Figs. S2b-6b** that only compounds **1** and **6** emitted strong fluorescence while the other four compounds (**2-5**) showed noisy PL signals without discernable peaks under the same measurement conditions. The emission peak of compound **1** located at from 425 nm to 450 nm in different polarity solvents, which could be assigned to the ICT emission [27]. While the compound **6** emitted two fluorescence peaks located at ~500 nm and ~530 nm in different polarity solvents, which could be assigned to the ICT emission and excited state intramolecular proton transfer (ESIPT) emission [28], respectively. The result stated that fine adjustment of the acceptor moieties could control the fluorescence emission in the series compounds. To further investigate the influence of different electron acceptors on charge transfer of the six compounds, time-dependent density functional theory (TDDFT) was carried on to investigate the electron cloud density distribution of the ground and excited states. The Gaussian 03 program and B3LYP/6-31G basis sets were used for calculations, then the isosurfaces of the highest occupied and the lowest unoccupied molecular orbital (HOMO and LUMO) were shown in **Fig. 5**. It could be seen that all the six compounds produced ICT progress upon photoexcitation, the HOMO and LUMO of compounds **1-4** were obviously dominated by the orbitals from the donor (carbazole ring) and the acceptor (Schiff base moieties), respectively, while that of the compounds **5** and **6** were inconspicuous due to the decrease of the electron-withdrawing ability of the acceptor caused by the introduction of diethylamino group. The calculation results illustrated the existence of the ICT progress and were accord with the absorption spectra, but could not explain why the compounds **2, 3, 4** and **5** were nonluminous in solution and compounds **1** and **6** were luminous. Hence, we tried to explain the difference of their fluorescence emission abilities from the molecular configuration calculated by crystal structure and found that the carbazole ring deviated the plane of the styrene obviously in compounds **1**, **2**, **3**, **5** and **6** with a dihedral angle of 62.274(24), 58.199(104), 59.134(108),63.418(156) and 65.784(130) and the Schiff base moieties in compounds **1**, **2** and **3** deviated the plane of the styrene with a dihedral angle of 52.885(101), 39.404(182), and 36.185(159), respectively, which showed the carbazole ring and the Schiff base moieties were not conjugate with the styrene well and could rotate freely. The rotation of aromatic rings could consume energy which resulted in the fluorescence quenching. While in compound **1**, the existence of the H···H interactions could connect two adjacent molecules into a dimer which adopted *J*-aggregation and restricted the rotations of the two terminal aromatic rings around the single bond. The same situations in the other compounds were not observed, which could be explain why the compound **1** could emit fluorescence in solution. Whereas for compound **6**, the carbazole ring contributed less to the energy levels and the electron densities were mainly located on the styrene, meanwhile, the existence of ESIPT could also explain the emission peak at long wavelength, thus compound **6** could emit fluorescence in solution.

4 Aggregation-induced emissions

As the six compounds are non-luminous or weak luminous in solution, meanwhile they are all insoluble in water but soluble in organic solvents such as acetonitrile, we determined the absorption and emission spectra of the diluted solutions or suspensions of the compounds **1-6** in acetonitrile-water mixtures with different water fractions (f_w, the volume percentage of water in organic-water mixtures) that can adjust the solvent polarity subtly. This is revealed by the images in **Figs. 6-7** and Figs. **S7-10**. As all the six compounds possess similar absorption and fluorescence emission properties in acetonitrile-water mixture solutions, we just used compound **1** as example to discuss in detail.

The absorption spectrum of compound **1** (20 μM) has been recorded and is shown in **Fig.6a**. We can see that compound **1** shows two absorption peaks in dilute acetonitrile solution which locates at ~293 nm and ~350 nm. Meanwhile, the spectra of the mixtures with high f_w (≥70%) values start to show level-off tails in the long wavelength region caused by the Mie scattering effect, which was suggested the formation of nanoaggregates [29]. As can be seen from the **Fig. 7** and **Figs. S7-9**, the other five compounds also showed similar characteristic of absorption spectrum with compound **1** under aggregation state.

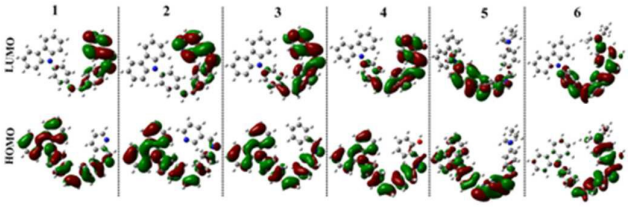

Fig. 5. Electron cloud distributions of compounds **1-6** calculated by the B3LYP/6-31G program.

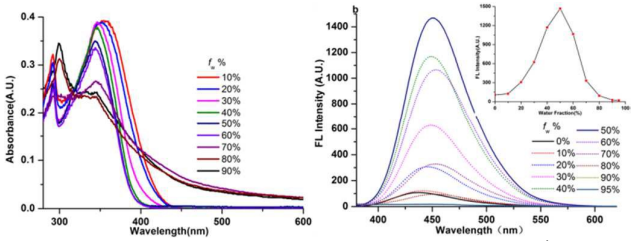

Fig. 6. Absorption (a) and fluorescence (b) spectra of compound **1** in water/acetonitrile mixtures with different f_w at 2.0×10^{-5} M.

View Article Online
DOI: 10.1039/C6OB02181F

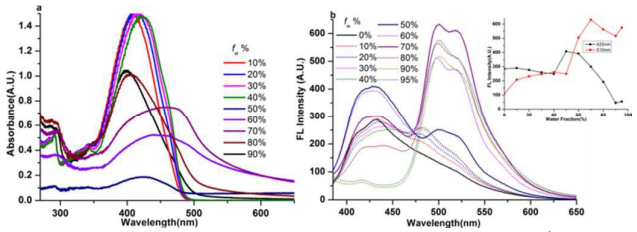

Fig. 7 Absorption (a) and fluorescence (b) spectra of compound **6** in water/acetonitrile mixtures with different f_w at 2.0×10^{-5} M.

The fluorescence spectrum of compounds **1** (20 μM) in the water-acetonitrile mixtures with different water contents were shown in **Fig 6b**, which showed obvious AIE properties, the fluorescence intensity primarily increased with the f_w increasing when f_w≤50%, and the highest fluorescence intensity at f_w = 50% was higher about 17.5-fold than that in the pure acetonitrile solution. Then decreased with the f_w increasing when f_w>50%, the inset depicts the changes of integrated intensity with different water fractions. The fluorescence spectra (**Figs. S7-9**) of compounds **2, 3** and **5** (20 μM) in the water-acetonitrile mixtures were similar with that of compound **1,** their fluorescence maxima reached at f_w = 50%, 30%, 20%, respectively.

The fluorescence spectrum of compounds **4** and **6** (20 μM) in water-acetonitrile mixtures with different water contents showed different feature with that of compounds **1**, **2, 3** and **5** which were depicted in **Fig. 7b** and **Figs.S9b**. It could be seen from **Fig.7b** that the two emission peaks of compound **6** both changed with the increasing of the water fractions, the high energy emission peak located at 425nm which was attributed to the ICT emission gradually increased with the increasing of water content when f_w≤50%, then decreased with the increasing of water content when f_w≥50%, while the low energy emission peak located at 510nm which was attributed to the ESIPT emission increased with the increasing of water content and reached its maxima at f_w=70%, then decreased gradually with the water fraction increasing. Meanwhile, the latter split into two peaks little by little. The result showed that both the two emission peak which generated from different energy level could be affected by the aggregation progress, while the ESIPT emission was stronger than the ICT emission at high water content perhaps due to the more water molecules was in solution, the easier the ESIPT progress generated. The compound **4** also showed similar characteristic of fluorescence emission spectrum with compounds **6** under aggregation state.

5 Mechanisms of AIE

To gain further insight into the influence of morphology on AIE properties, we also carried on the scanning electron microscope (SEM) tests for compounds **1-6** at different water fractions. The SEM images of compounds **1-6** were depicted in **Fig. 8**, we could see that the aggregates were formed as cubic nanoparticles in the mixture solution of compounds **1-3** and clubbed nanoparticles in the mixture solution of compounds **4-6** when reached their fluorescence maxima, respectively, while unordered aggregates appeared in the mixture of f_w = 90%.

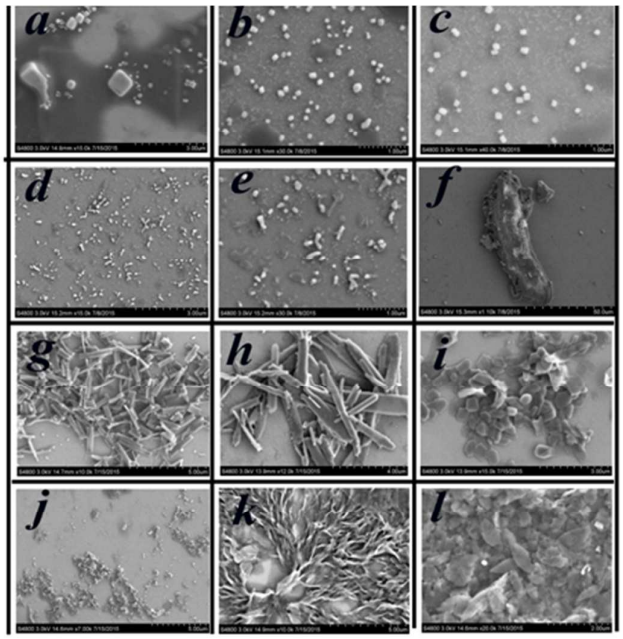

Fig. 8 SEM images of compounds **1-6** (20 μM) in acetonitrile/water mixtures with different water fractions: (a) **1** in acetonitrile/water (50/50 v/v); (b) **2** in acetonitrile /water (50/50 v/v); (c) **3** in acetonitrile /water (70/30 v/v); (g) **4** in acetonitrile /water (70/30 v/v); (h) **5** in acetonitrile /water (80/20 v/v); (i) **6** in acetonitrile /water (30/70 v/v); (d, e, f, j, k, l) compounds **1-6**, respectively, in acetonitrile /water (10/90 v/v).

The results illustrated ordered aggregation had important influence on the emission in aggregates. The reason may be that the weak intermolecular interactions could work efficiently under ordered aggregation condition, while under inordinate aggregation condition, some weak interactions such as C-H···π and H···H interactions, could not work effectively due to they asked for the periodical orientation of molecules. From the theoretical calculations, we could see that the compounds **1-4** owned ICT progress which generated from the donor (carbazole ring) to the acceptor (Schiff base moieties) through π-bridge (styrene), while that in compound **5** was from carbazole to styrene and in compound **6** was from Schiff base moieties to styrene, respectively. The result illustrated that the carbazole ring and Schiff base moieties hold important contribution to the energy level of molecule orbital. Whereas in crystal structure, multiple intermolecular interactions especially for C-H···π interactions came from the carbazole ring restricted the rotation of terminal groups including carbazole ring and Schiff base moieties, thereby, all the six compounds possessed AIE performance in aggregation state. In one word, the existence of C-H···π interactions generated from carbazole rings which was a common structure in all the six compounds played significant role in producing AIE properties. These findings could be provided reference to design new AIE compounds.

6 Cytotoxicity tests

Cytotoxicity was a potential side effect of compounds that must be controlled when dealing with living cells or tissues.

View Article Online
DOI: 10.1039/C6OB02181F

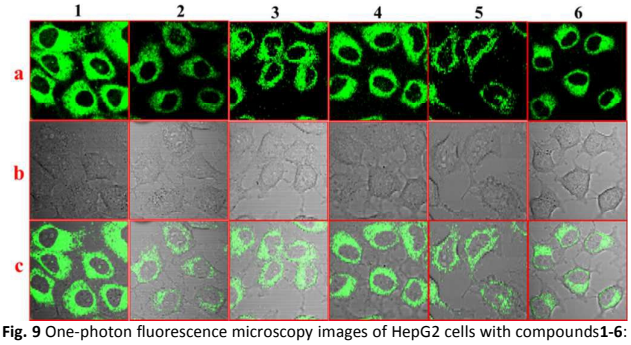

Fig. 9 One-photon fluorescence microscopy images of HepG2 cells with compounds**1-6**: (a) Dark-Field images, (b) Bright-field images, (c) Merged images.

Considering their application in cell imaging, the MTT assay [30-31] was performed to ascertain the cytotoxic effect of compounds 1-6 against Hela cells over a period of 24 h. **Fig. S11** showed the cell viability for Hela cells treated with compounds 1-6 at different concentrations. The results clearly indicated that no obvious cell viability decreased, even when the concentrations of the compounds reached up to 20 μM, the cell viability was still greater than 80%. The low cytotoxicity of the target compounds over a period of at least 24 h indicated it was suitable for cellular imaging applications. This is an important factor in further potential live cell imaging applications due to their relatively low cytotoxicity.

7 Bio-imaging

To explore the application for the six AIE compounds, the bio-imaging experiments were carried out by confocal laser scanning microscopy using HepG2 (human liver cancer cells) as an example, the tested compounds were dissolved in DMSO and then serially diluted in complete culture medium. Then we carried out bio-imaging studies in living HepG2 cells stained with compounds **1-6** by one photon microscopy. The excitation wavelength was fixed at their optimal excitation wavelength in one-photon microscopy imaging, respectively. As shown in **Fig. 9**, bright green fluorescence with similar intensity from the cells indicated that all the six compounds could be effectively internalized by HepG2 cells. The six compounds all went through the membrane and localized uniformly in the cytoplasm, which suggested that only the cell cytoplasm could be labelled by these compounds.

Conclusions

In this work, we reported a series of carbazole Schiff base dipole molecules to realize AIE performance through the restriction of terminal groups which caused by the multiple weak interactions generated from the carbazole ring and Schiff base moieties. The existence of the H···H interactions and C-H···π interactions played significant role on their luminescence properties in solution and/or aggregation state, especially for the dihydrogen bonds, which not only contributed for the fluorescence emission of compound **1** in pure acetonitrile solution, but also in favor of AIE. The structure-property relationship was summarized clearly and all the results displayed that the carbazole ring could generate multiple weak interactions effectively, which could provide reference for designing new AIE compounds.

Experimental sections

1. General procedures

All commercially available chemicals were of analytical grade. Every solvent was purified as conventional methods beforehand. ^{1}H and ^{13}C NMR spectra were recorded on a Bruker AV 400 Ultrashield spectrometer using dimethylsulfoxide-d_6 (DMSO-d_6) or CD_3COCD_3 as solvent. Chemical shifts were reported in parts per million (ppm) relative to internal TMS (0 ppm) and coupling constant in Hz. Splitting patterns were described as singlet (s), doublet (d), triplet (t), quartet (q), or multiplet (m). IR spectra were recorded with a Nicolet FT-IR S10 spectrometer (ATR model) in the 4000 - 525 cm^{-1} region. Melting points (uncorrected) were determined on a XT4 MP apparatus (Taike Corp., Beijing, China). The mass spectra were obtained on a LTQ-Orbitrap XL mass spectrometer. The X-ray diffraction measurements were performed on a CCD area detector using graphite monochromated MoKa radiation (λ = 0.71069 Å) at 298 (2) K. Intensity data were collected in the variable ω/2θ-scan mode. The structures were solved by direct methods and difference Fourier syntheses. The non-hydrogen atoms were refined anisotropically and hydrogen atoms were introduced geometrically. Calculations were performed with SHELXTL-97 program package. Crystallographic data for the structures reported in this paper have been deposited with the Cambridge Crystallographic Data Centre as supplementary publication no. CCDC: 1040856 (for **1**), 1487391 (for **2**), 1040859 (for **3**), 1040861 (for **5**) and 1040862 (for **6**), respectively.

2. Optical measurements

The one-photon absorption (OPA) spectra were recorded on the UV-3600 spectrophotometer. The one-photon emission fluorescence (OPEF) spectra were performed using a Hitachi F-7000 fluorescence spectrophotometer. In the measurements of emission and excitation spectra, the pass width was 10 nm for all compounds. OPA and OPEF of Compounds **1 - 6** were measured in six organic solvents with different polarities at the concentration of 2×10^{-5} mol L^{-1}. The quartz cuvettes used were of 1 cm path length.

3. Cytotoxicity assays in cells

To ascertain the cytotoxic effect of the six compounds, the 3-(4, 5 - dimethylthiazol - 2 - yl) - 2, 5 - diphenyltetrazolium bromide (MTT) assay was performed. HepG2 cells were trypsinized and plated to ~70% confluence in 96 - well plates 24 h before treatment. Prior to the compounds' treatment, the dulbecco's modified eagle medium (DMEM) was removed and replaced with fresh DMEM, and aliquots of the compound stock solutions (1 mM DMSO) were added to obtain final concentrations of 5, 10, 20, 40 and 60 mM. The treated cells were incubated for 24 h at 37℃ and under 5% CO_2.

View Article Online
DOI: 10.1039/C6OB02181F

Subsequently, the cells were treated with 5 mg / mL MTT (40 μL/well) and incubated for an additional 4 h (37 ℃, 5% CO_2). Then, DMEM was removed, the formazan crystals were dissolved in DMSO (150 μL/well), and the absorbance at 570 nm was recorded. The cell viability (%) was calculated according to the following Equation:

Cell Viability% = OD570 (sample) / OD570 (control) × 100

Where OD570 (sample) represents the optical density of the wells treated with various concentration of the compounds and OD570 (control) represents that of the wells treated with DMEM + 10% fetal calf serum (FCS). Three independent trials were conducted, and the averages and standard deviations are reported. The reported percent cell survival values are relative to untreated control cells.

4 Cell Image

HepG2 cells were seeded and grown in 6 well plates at a density of 2×10^5 cells per well for 96 h. For live cell imaging, cell cultures were incubated with the complexes (PBS : cell media = 1 : 9) at concentrations 20 μM and maintained at 37 °C in an atmosphere of 5% CO_2 and 95% air for incubation times ranging for 2 h. Then the cells were washed with PBS (3 × 3 mL per well) and 3 mL of PBS was added to each cell. The cells were imaged using confocal laser scanning microscopy and water immersion lenses, then the fluorescence emission measured at 520-560 nm with optimal excitation energy.

5. Synthesis and characterization

5.1. Synthesis of the intermediate 1-4

Intermediate **1**, intermediate **2**, intermediate **3** and intermediate **4**, were synthesized according to the methods reported in the literature [12] with some modifications.

5.2. Synthesis of Compounds 1 - 6

Intermediate **4** (0.5 g, 1.4 mmol) were dissolved in 60 mL of methanol and stirred for 10 min. Then glacial acetic acid was added in catalytic amount (3 drops) and corresponding aldehyde (1.8 mmol) was added dropwise to the reaction system, the reaction mixture was refluxed at 65 °C for 2 h. After the reaction finished, the mixture was immediately filtered under reduced pressure and recrystallization used methanol to obtain pure product.

Compound **1**, 4-((E)-4-(9H-carbazol-9-yl)styryl)-N-(pyridin-2-ylmethylene) aniline, yellow powder, 0.41 g, yield: 59 %, melting point: 206.5-207.4 °C. FT- IR (ATR, cm^{-1}): 1595.48 (w), 1515.26 (m), 1479.07 (w), 1451.52 (s), 1435.11 (m), 1365.23 (m), 1335.10 (m), 1316.28 (m), 1230.84 (s), 1184.19 (w), 950.82 (w), 832.65 (m), 746.57 (s), 723.20 (s), 623.81 (m). ^{1}H NMR (400 MHz, DMSO-d_6, δ): 8.75 - 8.74 (1 H, d, *J* = 4.0), 8.68 (1 H, s), 8.27 - 8.26 (2 H, d, *J* = 4.0), 8.20 -8.18 (1 H, d, *J* = 8.0), 8.00 - 7.96 (1 H, t, *J* = 8.0, 8.0), 7.94 - 7.91 (2 H, d, *J* = 12.0), 7.77 - 7.75 (2 H, d, *J* = 8.0), 7.67 - 7.65 (2 H, d, *J* = 8.0), 7.56 - 7.54 (1 H, m), 7.45 - 7.43 (8 H, m), 7.32 - 7.29 (2 H, m). ^{13}C NMR (100 MHz, DMSO-d_6, δ): 160.33, 154.06, 149.72, 139.98, 137.07, 135.94, 135.76, 127.62, 127.52, 126.81, 126.27, 125.65, 121.84, 121.23, 120.53, 120.10, 113.83, 109.70. MS (ESI) *m/z*: found, $[M+H]^+$, 450.1981; molecular formula $C_{32}H_{23}N_3$ requires $[M+H]^+$, 450.1971.

Compound **2**, 4-((E)-4-(9H-carbazol-9-yl)styryl)-N-(pyridin-3-ylmethylene) aniline, yellow powder, 0.46 g, yield: 74 %, melting point: 186.1-187.2 °C. FT- IR (ATR, cm^{-1}): 1625.21 (w), 1595.16 (w), 1514.53 (m), 1478.98 (m), 1451.01 (s), 1335.15 (m), 1316.23 (m), 1231.16 (m), 1183.27 (m), 1119.07 (m), 1016.23 (m), 991.81 (m), 833.42 (m), 747.91 (s), 722.00 (s). ^{1}H NMR (400 MHz, DMSO-d_6, δ): 9.09 (1 H, s), 8.81 (1 H, s), 8.73 - 8.72 (1 H, d, *J* = 4.0), 8.36 - 8.34 (1 H, d, *J* = 8.0), 8.28 - 8.26 (2 H, d, *J* = 8.0), 7.93 - 7.91 (2 H, d, *J* = 8.0), 7.77 - 7.75 (2 H, d, *J* = 8.0), 7.65 - 7.63 (2 H, d, *J* = 8.0), 7.56 - 7.53 (1 H, m), 7.45 - 7.39 (8 H, m), 7.31 -7.29 (2 H, m). ^{13}C NMR (100 MHz, DMSO-d_6, δ): 158.13, 154.57, 151.94, 150.45, 139.98, 136.37, 135.91, 135.41, 134.96, 131.58, 128.01, 127.36, 126.27, 124.08, 122.74, 121.74, 120.53, 120.10, 113.93, 109.70. MS (ESI) *m/z*: found, $[M+H]^+$, 450.1987; molecular formula $C_{32}H_{23}N_3$ requires $[M+H]^+$, 450.1971.

Compound **3**, 4-((E)-4-(9H-carbazol-9-yl)styryl)-N-benzylide--neaniline, deep yellow powder,0.40 g, yield: 64 %, melting point: 233.3-234.6 °C. FT- IR (ATR, cm^{-1}): 1594.96 (m), 1512.72 (m), 1478.12 (w), 1449.34 (s), 1408.15 (w), 1334.77 (w), 1315.75 (m), 1227.11 (s), 1102.84 (w), 961.86 (m), 839.33 (s), 748.65 (s), 723.67 (s). ^{1}H NMR (400 MHz, DMSO-d_6, δ): 8.71 (1 H, s), 8.27-8.25 (2 H, d, *J* = 8.0), 8.03 - 7.87 (4 H, m), 7.81 - 7.21 (17 H, m). ^{13}C NMR (100 MHz, DMSO-d_6, δ): 160.38, 150.76, 140.05, 128.91, 128.68, 128.69, 128.05, 127.69, 127.17, 126.83, 126.27, 122.91, 121.67, 120.57, 120.06, 109.71. MS (APCI) *m/z*: found, $[M+H]^-$, 449.2031; molecular formula $C_{32}H_{23}N_3$ requires $[M+H]^-$, 449.2018.

Compound **4**, 2-(((4-((E)-4-(9H-carbazol-9-yl)styryl)phenyl)i--mino)methyl) phenol, yellow powder, 0.43 g, yield: 67 %, melting point: 251.2-252.2 °C. FT- IR (ATR, cm^{-1}): 3023.25 (w), 1594.96 (m), 1512.72 (m), 1478.12 (m), 1449.34 (s), 1334.77 (m), 1227.11 (m), 1183.33 (w), 961.86 (m), 839.33 (s), 748.65 (s), 723.67 (s). (0.43 g, yield: 66.7 %,): ^{1}H NMR (400 MHz, DMSO-d_6, δ): 13.13 (1H, s), 9.04 (1H, s), 8.27-8.25 (2H, d, *J* = 8.0), 7.93-7.91 (2H, d, *J* = 8.0), 7.79-7.77 (2H, d, *J* = 8.0), 7.69-7.66 (3H, dd, *J* = 12.0), 7.55 - 7.37 (9H, m), 7.41 -7.30 (2H, m), 7.00 - 6.98 (2H, m). ^{13}C NMR (100 MHz, DMSO-d_6, δ): 163.45, 160.82, 156.94, 147.76, 140.52, 132.97, 130.54, 129.10, 128.61, 128.21, 127.25, 126.69, 123.23, 122.40, 121.06, 120.59, 119.95, 119.61, 117.09, 110.11. MS (ESI) *m/z*: found, $[M+H]^+$, 465.1980; molecular formula $C_{33}H_{24}N_2O$ requires $[M+H]^+$, 465.1968.

Compound **5**, 4-(((4-((E)-4-(9H-carbazol-9-yl)styryl)phenyl)i--mino)methyl)-N,N-diethylaniline, yellow powder, 0.50 g, yield: 69 %, melting point: 209.1-211.4 °C. FT- IR (ATR, cm^{-1}): 3023.25 (w), 1616.36 (m), 1596.10 (m), 1514.46 (m), 1450.03 (s), 1359.65 (m), 1334.89 (m), 1279.58 (m), 1226.06 (m), 1170.21 (m), 1152.14 (m), 964.96 (m), 835.66 (m), 746.93 (s), 721.95 (s). ^{1}H NMR (400 MHz, DMSO-d_6, δ): 8.45 (1 H, s), 8.27 - 8.25 (2 H, d, *J* = 8.0), 7.91-7.89 (2 H, d, *J* = 8.0), 7.75-7.73 (2 H, d, *J* = 8.0), 7.69-7.63 (4 H, dd, *J* = 8.0, 8.0), 7.74 - 7.24 (10 H, m), 6.77-6.75 (2 H, d, *J* = 8.0), 3.46-3.41 (4 H, m), 1.16-1.13 (6 H, t, *J* = 8.0). ^{13}C NMR (100 MHz, CD_3COCD_3, δ): 159.31, 131.33, 130.21, 129.65, 128.24, 127.87, 127.23, 126.83, 126.23, 121.62, 114.58, 110.81, 110.11, 44.19, 11.65. MS (ESI) *m/z*: found, $[M+H]^+$, 520.2767; molecular formula $C_{37}H_{33}N_3$ requires $[M+H]^+$, 520.2753.

View Article Online
DOI: 10.1039/C6OB02181F

Compound **6**, 2-(((4-((E)-4-(9H-carbazol-9-yl)styryl)phenyl)i--mino)methyl)-5-(diethylamino)phenol, yellowish-brown powder, 0.52 g, yield: 70 %, melting point: 243.5-246.0 °C. FT-IR (ATR, cm^{-1}): 2970.10 (w), 1573.78 (m), 1548.20 (m), 1515.57 (s), 1479.27 (m), 1450.34 (s), 1358.36 (m), 1314.66 (m), 1266.93 (m), 1231.03 (m), 1149.36 (m), 962.88 (m), 835.54 (m), 817.36 (m), 748.64 (s), 722.825 (s). (0.52 g, yield: 70.0 %,): ^{1}H NMR (400 MHz, DMSO-d_6, δ): 13.70 (1 H, s), 8.77 (1 H, s), 8.27-8.25 (2 H, d, *J* = 8.0), 7.92-7.90 (2 H, d, *J* = 8.0), 7.70-7.68 (2 H, d, *J* = 8.0), 7.66-7.64 (2 H, d, *J* = 8.0), 7.45 - 7.31 (11 H, m), 6.35-6.33 (1 H, d, *J* = 8.0), 6.08 (1 H, s), 3.44-3.38 (4 H, m), 1.15-1.12 (6 H, t, *J* = 6.0). ^{13}C NMR (100 MHz, CD_3COCD_3, δ): 161.52, 141.43, 134.99, 134.30, 129.11, 127.98, 127.78, 127.45, 126.88, 126.10, 120.60, 109.68, 103.74, 97.63, 44.32, 12.10. MS (APCI) *m/z*: found, $[M+H]^+$, 536.2712; molecular formula $C_{37}H_{33}N_3O$ requires $[M+H]^+$, 536.2703.

Acknowledgements

This work was supported by General Program of National Natural Science Foundation of China (21271003, 21271004, 51432001 and 51472002), Science and Technology Plan of Anhui Province (1604b0602016), the National Science and technology support project (2014BAK09B00), the Natural Science Foundation of Anhui Province (*1608085MB26*), the Natural Science Foundation of Education Committee of Anhui Province (KJ2016A218) and the Youth Fund of Anhui Agriculture University (2015ZD08).

Notes and references

1 J. Zhou, Q. Liu, W. Feng, Y. Sun and F. Li, *Chem. Rev.*, 2014, **115**, 395-465.
2 K. Brunner, A. Van Dijken, H. Börner, J. Bastiaansen, N. Kiggen and B. Langeveld, *J. Am. Chem. Soc.,* 2004, **126**, 6035-6042.
3 G. Qian, Z. Zhong, M. Luo, D. Yu, Z. Zhang, Z. Wang and D. Ma, *Adv. Mater.,* 2009, **21**, 111-116.
4 Y. Ooyama, G. Ito, K. Kushimoto, K. Komaguchi, I. Imae and Y. Harima, *Org. Biomol. Chem.*, 2010, **8**, 2756-2770.
5 P. Ledwon, W. Kuznik, M. Lapkowski and M. Majchrzak, *New J Chem.*, 2012, **36**, 2347-2352.
6 C. Qin, M. Zhou, W. Zhang, X. Wang and G.Chen, *Dyes Pigments*, 2008, **77**, 678-685.
7 G. He, L. Yuan, Y. Cui, M. Li and P. Prasad, *J Appl. Phys.*, 1997, **81**, 2529-2537.
8 D. Cvejn, S. Achelle, O. Pytela, J. Malval, A. Spangenberg, N. Cabon and F. Robin-Le Guen, *Dyes Pigments*, 2016, **124**, 101-109.
9 C. Lavanya Devi, K. Yesudas, N. Makarov, V. Rao, K. Bhanuprakash and J. Perry, *Dyes Pigments*, 2015, **113**, 682-691.
10 (a) Y. Hong, J. Lam and B. Tang, *Chem. Commun.*, 2009, **29**, 4332-4353. (b) Y. Hong, J. Lam and B. Tang, *Chem. Soc. Rev.*, 2011, **40**, 5361-5388.
11 K. Upamali, L. Estrada, P. De, X. Cai, J. Krause and D. Neckers, *Langmuir*, 2011, **27**, 1573-1580.
12 M. D. Yang, D. L Xu, W. G. Xi, L. Wang, J. Zheng, J. Huang and Y. P. Tian, *J Org. Chem.*, 2013, **78**, 10344-10359.
13 L. Yang, W. J. Zhu, M. Fang, Q. Zhang and C. Li, *Spectrochim. Acta. A*, 2013, **109**, 186-192.
14 S. Kim, S. Byeon, S. Hwang and J. Lee, *Chem. Commun.*, 2015, **51**, 10672-10675.
15 P. Xue, J. Sun, P. Chen, P. Wang, B. Yao, P. Gong and R. Lu, *Chem. Commun.,* 2015, **51**, 10381-10384.
16 H. Wang, Q. Zhang, J. Zhang, L. Li, Q. Zhang, S. Li, S. Zhang, J. Wu and Y. Tian, *Dyes Pigments*, 2014, **102**, 263-272.
17 Y. Li, Q. Guo, Z. Li, J. Pei and W.Tian, *Enegr. Environ. Sci.*, 2010, **10**, 1427-1436.
18 X. Lou, Z. Zhao, Y. Hong, C. Dong, X. Min, Y. Zhuang and B. Tang, *Nanoscale*, 2014, **6**, 14691-14696.
19 P. Popelier, *J Phys. Chem. A*, **1998**, 102, 1873-1878.
20 D. A. Safin, M. G. Babashkina, K. Robeyns, M. P. Mitoraj, P. Kubisiak and Y. Garcia, *Chem-Eur. J,* 2015, **21**, 16679-16687.
21 W. T. Klooster, T. F. Koetzle, P. E. M. Siegbahn, T. B. Richardson and R. H. Crabtree, *J. Am. Chem. Soc.*, 1999, **27**, 6337-6343.
22 P. Lipkowski, S. Grabowski, T. Robinson and J. Leszczynski, *The J Phys. Chem. A*, 2004, **108**, 10865-10872.
23 V. Bakhmutov, John Wiley & Sons, 2008.
24 R. Crabtree, *Science*, 1998, **282**, 2000-2001.
25 S. Grabowski, *Chem. Phys. Lett.*, 2000, **327**, 203-208.
26 Z. Zheng, H. P. Zhou, G. Y. Xu, Z. Yu, X. Yang, L. Cheng and Y. P. Tian, *Tetrahedron*, 2012, **68**, 6569-6574.
27 H. P. Zhou, Z. Zheng, G. Xu, Z. Yu, X. Yang, L. Cheng and Y. P. Tian, *Dyes Pigments*, 2012, **94**, 570-582.
28 K. Zheng, W. Lin, L. Tan, H. Chen and H. Cui, *Chem. Sci.*, 2014, **9**, 3439-3448.
29 A. Kulkarni, X. Kong and S. Jenekhe, *Adv. Funct. Mater.,* 2006, **16**, 1057-1066.
30 Y. Shigemitsu, T. Mutai, H. Houjou and K, *J Phys. Chem. A*, 2012, **116**, 12041-12048.
31 X. P. Gan, Y. Wang, X. P. Ge, W. Li, X. Zhang, W. Zhu, H. P. Zhou, J. Y. Wu and Y. P. Tian, *Dyes Pigments*, 2015, 120, 65-73.